Neurochemistry International 182 (2025) 105906

Contents lists available at ScienceDirect

Neurochemistry International

journal homepage: www.elsevier.com/locate/neuint

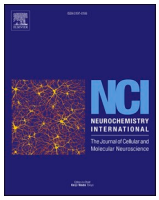

Accelerated senescence exacerbates α-synucleinopathy in senescence-accelerated prone 8 mice via persistent neuroinflammation

Hiroshi Sakiyama [a,1], Kousuke Baba [a,b,1,*], Yasuyoshi Kimura [a], Kotaro Ogawa [a], Ujiakira Nishiike [a], Hideki Hayakawa [a], Miki Yoshida [a], Cesar Aguirre [a], Kensuke Ikenaka [a], Seiichi Nagano [a,b], Hideki Mochizuki [a,**]

[a] Department of Neurology, Osaka University, Graduate School of Medicine, Osaka, Japan
[b] Department of Neurotherapeutics, Osaka University Graduate School of Medicine, Osaka, Japan

ARTICLE INFO

Keywords:
Parkinson's disease
α-synucleinopathy
Neuroinflammation
Senescence-accelerated prone 8 (SAMP8) mice
CC-Chemokine ligand 21

ABSTRACT

Parkinson's disease (PD) is characterized by the formation of α-synuclein (α-syn) aggregates, which lead to dopaminergic neuronal degeneration. The incidence of PD increases with age, and senescence is considered to be a major risk factor for PD. In this study, we evaluated the effect of senescence on PD pathology using α-synuclein preformed fibrils (PFF) injection model in senescence-accelerated mice. We injected PFF into the substantia nigra (SN) of senescence-accelerated prone 8 (SAMP8) mice and senescence-accelerated resistant 1 (SAMR1) mice. At 24 weeks after injection of saline or PFF, we found that SAMP8 mice injected with PFF exhibited robust Lewy pathology and exacerbated degeneration of dopaminergic neurons in the SN compared to PFF-injected SAMR1 mice. We further observed an increase in the number of Iba1-positive cells in the brains of PFF-injected SAMP8 mice. RNA sequencing revealed that several genes related to neuroinflammation were upregulated in the brains of PFF-injected SAMP8 mice compared to SAMR1 mice. Inflammatory chemokine *CC*-chemokine ligand 21 (CCL21) was upregulated in PFF-injected SAMP8 mice and expressed in the glial cells of these mice. Our research indicates that accelerated senescence leads to persistent neuroinflammation, which plays an important role in the exacerbation of α-synucleinopathy.

1. Introduction

Parkinson's disease (PD) is a common neurodegenerative disorder characterized by the degeneration of dopaminergic neurons in the substantia nigra (SN) and accumulation of α-synuclein (α-syn) forming Lewy bodies (LB) and Lewy neurites (LN) (Spillantini et al., 1997). The mechanism of PD is pathological spreading of α-syn and the pathological α-syn seeds aggregation of soluble α-syn (Wood S.J. et al., 1999). The pathological α-syn is incorporated into endosomes, where it can encounter endogenous soluble α-syn. It serves as a template for the conversion of soluble α-syn, and the misfolding of monomers is amplified. The amplified pathological α-syn is released into the cytoplasm upon endosomal rupture, where it acts as a seed for further aggregation of α-syn in the cytoplasm (Tofaris G.K. et al., 2017). Idiopathic PD is a multifactorial disease caused by genetic and environmental factors (Wirdefeldt et al., 2011). The prevalence of PD has globally increased with aging (Ray Dorsey et al., 2018), and numerous epidemiological studies have revealed a correlation between aging and the incidence of PD. According to a meta-analysis comprising 47 epidemiologic studies, the incidence of PD increases with age and is approximately 10-fold higher among 80-, than 50-year-old persons (Pringsheim et al., 2014). Kempster et al. reported that the time of progression from disease onset to advanced stage in patients with early-onset PD was considerably longer than in patients with older-onset PD (Kempster et al., 2010). This result could also be interpreted as younger-onset PD progressing more slowly, and older-onset PD progressing more rapidly. In other words, "senescence," which refers to the deterioration of biological functions, could be a higher risk factor for PD progression than "aging," which refers to the passage of time.

Cellular senescence causes neuroinflammation, mitochondrial

* Corresponding author. Department of Neurology, Osaka University, Graduate School of Medicine, Osaka, Japan.
** Corresponding author.
E-mail addresses: babablanc@gmail.com (K. Baba), hmochizuki@neurol.med.osaka-u.ac.jp (H. Mochizuki).
[1] These authors have contributed equally to this work and share first authorship.

https://doi.org/10.1016/j.neuint.2024.105906
Received 29 September 2024; Received in revised form 13 November 2024; Accepted 21 November 2024
Available online 23 November 2024

dysfunction, and loss of proteostasis, contributing to neurodegenerative diseases, including PD (Barrientos et al., 2015; Kaushik and Cuervo, 2015; Bose and Beal, 2016). Senescent cells such as glial cells, endothelial cells, and neurons can aberrantly activate their secretory function, releasing pro-inflammatory cytokines. This activation contributes to the progression of neurodegenerative diseases (Martínez-Cué and Rueda, 2020). Indeed, senescence markers p16 and senescence-associated secretory phenotype (SASP) factors such as IL-6, IL-1α, IL-8, and MMP-3 are increased in brain tissues of PD as compared to age-matched controls (Mogi et al., 1994; Chinta et al., 2018). Additionally, senescent cells disrupt proteostasis, accumulating misfolded or abnormal proteins such as α-syn, a characteristic hallmark of PD (Rodriguez M et al., 2015). Moreover, senescence, associated with the accumulation of senescent cells, might play a significant role in the development of PD (Baker and Petersen, 2018). Overall, senescent cells and their associated effects, such as SASP, might function in the development of PD by affecting proteostasis and neuroinflammation. Based on these notions, it is crucial to examine whether a senescence accelerated state could affect the progression of α-synucleinopathy, the central pathological mechanism of PD. However, there are various limitations to investigating the effects of senescence on α-synucleinopathy using common mouse models such as C57BL/6 mice. In order to study the effects of senescence in these mice, it is necessary to obtain a large number of older mice, which is often a practical challenge.

Therefore, we used senescence-accelerated prone 8 (SAMP8) mice to elucidate the association between a senescence accelerated state and the progression of α-synucleinopathy. Senescence-accelerated mice (SAM) were derived from selective inbreeding on the AKR/J strain of mice, based on the grading score of senescence, life span and pathologic phenotypes. SAM mice are classified into senescence-accelerated mouse prone (SAMP) lines, which show accelerated senescence, and senescence-accelerated mouse resistant (SAMR) lines, which exhibit senescence at a natural pace. In previous studies, SAMP8 mice have been regularly used as a model to study brain aging and cognitive decline, and SAMR1 mice have been used as the appropriate control strain. (Akiguchi et al., 2017; Liu et al., 2020). Reale et al. demonstrated proteomic changes in the hippocampi of SAMP8 mice, suggesting the involvement of inflammatory cytokines in brain aging (Reale et al., 2022). Thus, SAMP8 mice offer a promising animal model for senescence-related research owing to their shorter observation period required for symptoms to become manifest, compared with standard wild type strains such as C57BL/6J mice. In this study, we adapted the G51D mutant α-syn preformed fibrils (PFF)-injected PD model, which demonstrated robust progressive Lewy pathology and subsequent dopaminergic neurodegeneration (Hayakawa et al., 2020) to SAMP8 and SAMR1 mice, and assessed the effects of senescence on α-synucleinopathy.

2. Material and methods

2.1. Purification of the G51D mutant α-syn and preparation of PFF

Human G51D mutant α-syn was purified from Escherichia coli (*E. coli*) as described previously (Yagi et al., 2005). Briefly, a plasmid containing human G51D α-syn was expressed in *E. coli* BL21 (DE3) cells (Novagen, Merck, CA, USA). The cells were then suspended in purification buffer and disrupted by sonication. Streptomycin sulfate (2.5% w/w) was added to the supernatant, followed by centrifugation. The supernatant was precipitated by adding solid ammonium sulfate to 70% saturation, centrifuged, dialyzed overnight, applied to a Resource-Q column (GE Healthcare, Little Chalfont, UK) with 50 mM Tris-HCl buffer (pH 7.5), and eluted using a linear gradient of 0–1 M NaCl. α-syn-enriched fractions were purified by size exclusion chromatography using a Superdex 200 10/300 GL column (GE Healthcare).

PFF was generated by preparing solutions of monomeric α-syn at 5.0 mg/mL in phosphate-buffered saline ([PBS], 10 mM phosphates, 140 mM NaCl, 2.7 mM KCl, Takara, Shiga, Japan) in a total volume of 200 μL, with 1% seeding of PFF, and incubated at 37 °C, 800 rpm, for five days. Fibrils were centrifuged at 20 °C, 10,000×*g*, for 1 h, and the pellet was resuspended in PBS, and fragmented by ultrasonication to generate pathologic PFFs. To prepare PFF with uniform size, ultrasonication pulses of 2 s followed by 8 s quiescence using a UD-100 ultrasonic disruptor (Tomy Seiko, Tokyo, Japan) were applied to PFF, with a total incubation time of 20 min. PFF morphology was visualized using transmission electron microscopy ([TEM], Hitachi H-7650, Tokyo, Japan). PPF was aliquoted, stored at −80 °C, and used within 1 h after thawing at room temperature.

2.2. Animals

Eight-week-old male SAMR1 and SAMP8 mice were purchased from SLC (Japan SLC, Hamamatsu, Japan). The animals were kept under 12-h light/dark cycles and standard housing conditions with free access to food and water. They were allowed to acclimate for >1 week before the experiment. Mice were anesthetized via intraperitoneal injection of a combination anesthetic (0.3 mg/kg of medetomidine, 4.0 mg/kg of midazolam, and 5.0 mg/kg of butorphanol). Stereotaxic surgery was performed as follows: Mice underwent fixation using a conventional three-point fixation method involving a tooth-bar and earplugs. Following fixation, the skull was perforated using a drill, and unilateral injections of either saline (4 μL) or PFF (20 μg/4 μL) into the SN were administered (administration rate: 0.01 μl/s) using a Hamilton micro syringe (Hamilton, NV, USA). The coordinates used to locate the injection site were: 1.3 mm lateral, −2.8 mm posterior from the bregma, and 4.3 mm below the dural surface.

2.3. Immunohistochemistry

SAMR1 (N = 21), and SAMP8 (N = 17) mice were subjected to immunobiological analysis. At 24 weeks after injection, mice were deeply anesthetized and perfused transcardially with PBS and 4 % paraformaldehyde in PBS. The brains were removed, post-fixed overnight in 4 % paraformaldehyde in PBS, and then immersed in PBS containing 30 % sucrose until they sank.

Immunohistochemistry was performed on 20 μm serial sections obtained using a cryostat (CM1850; Leica Microsystems, Wetzlar, Germany). Serial sections were placed in a 24-well dish, with each well containing four sections. Antigen retrieval was performed by immersing the slides in 0.1 M sodium citrate buffer (pH 6) and heated them at 121 °C for 5 min. After the endogenous peroxidase activity was quenched with 3 % H2O2 for 10 min, the sections were washed with PBS three times for 5 min each and incubated overnight at 4 °C with 10% Block-Ace solution (KAC, Hyogo, Japan) and the following primary antibodies: anti-tyrosine hydroxylase ([TH], 1:5000, Calbiochem, MA, USA), anti-ionized calcium binding adaptor molecule 1 ([Iba1], 1:1000, Wako, Osaka, Japan), anti-phosphorylated α-syn ([p-α-syn], 1:1000, Wako, Osaka, Japan). The sections were washed with PBS (three times for 5 min each), and incubated for 1 h at room temperature with a biotinylated anti-rabbit IgG antibody (1:500, Vector Laboratories, CA, USA). After another wash with PBS (three times for 5 min each), the sections were treated for 1 h at room temperature with an avidin-biotin-peroxidase complex (Vector Laboratories, CA, USA). The reaction products were visualized in 5 min of incubation using 3,3′-diaminobenzidine tetrahydrochloride ([DAB], Sigma Aldrich, MO, USA).

Immunohistochemical images were obtained using an All-in-One Fluorescence Microscope BZ-X710 with BZ-X Analyzer Software (Keyence, Osaka, Japan). We quantified the area with phosphorylated α-syn (p-α-syn)-positive LN-like pathology and the Iba1-positive cells in the non-injected and the injected side of the SN. Three sections of the SN were selected from each animal, and measured area of SN according to the atlas. The images of the SN were obtained at three divisions at × 20 magnification with the same setting. The measurements were conducted using the BZ-H3C Hybrid Cell Count Software (Keyence, Osaka, Japan)

with the same settings. For stereological assessment of the total number of TH and Nissl double-immunopositive neurons, serial nigral sections were prepared. Every fourth section was stained through the entire extent of the SN. Cells were counted according to the method previously described (Hayakawa et al., 2020), and area of SN was measured according to the atlas.

2.4. Immunofluorescence staining

For immunofluorescence staining, we performed procedures similar to those described above for immunohistochemistry. The sections were washed with PBS and incubated overnight at 4 °C with the following primary antibodies: anti–CC–chemokine ligand 21 ([CCL21], 1:500, Pepro Tech, NJ, USA), anti-interferon regulatory factor 7 ([IRF7], 1:100, Proteintech, IL, USA), anti-glial fibrillary acidic protein([GFAP], 1:500, Abcam, Cambridge, UK), and anti-Iba1 (1:1000, Abcam). The sections were washed with PBS, and incubated for 1 h at room temperature with the following secondary antibodies: Alexa Fluor 488 (1:500, Abcam, Cambridge, UK), Alexa Flour 594 (1:500, Thermo Scientific, MA, USA), Alexa Fluor 488 (1:500, Thermo Scientific), Alexa Fluor 568 (1:500, Abcam), Cy3 (1:500, Jackson ImmunoResearch, PA, USA) and FITC (1:250, Jackson ImmunoResearch). The sections corresponding to the PFF-injected side of the SN were visualized using a spinning disk confocal microscope (Spin SR10, Olympus, Tokyo, Japan). We quantified CCL21-and Iba1-positive area, and the CCL21-and GFAP-positive area in the injected side of the SN. Three sections, including the SN according to Atlas, were selected per animal. Measurements were performed using ImageJ software (NIH, MD, USA). We selected type 8-bit, used the “adjust” and “threshold” at the same setting, and “measure” commands in ImageJ software.

2.5. Western blot analysis

SAMR1 (N = 12), and SAMP8 (N = 12) mice were subjected to Western blot analysis. At 24 weeks after injection, the mice were deeply anesthetized and perfused transcardially with PBS. The brains were removed immediately and sectioned into five serial 1 mm-thick coronal block slices using a mouse brain matrix (RBM-2000C; ASI Instruments, MI, USA). Brain samples, including the injected side of the SN were homogenized in CelLytic MT Mammalian Tissue Lysis Reagent (Sigma-Aldrich, MO, USA) with a protease inhibitor cocktail (1:100, Calbiochem, MA, USA) and a phosphatase inhibitor cocktail (1:100, Calbiochem). Lysates were then centrifuged at 15000 rpm for 20 min at 4 °C, and protein levels were determined with a BCA Protein Assay Kit (Thermo Scientific). Next, sodium dodecyl sulfate (SDS)-polyacrylamide gel electrophoresis (Wako) was performed at 10–20 % gradient, followed by the transfer of bands onto polyvinylidene difluoride membranes (Bio-Rad Laboratories, CA, USA). After blocking with 5 % skim milk for 1 h at room temperature, the membranes were incubated overnight at 4 °C with the following primary antibodies: anti-TH (1:10000, Calbiochem, MA, USA), anti-Iba1 (1:1000; Novus Biologicals, CO, USA) and anti-actin (1:25000, Millipore, MA, USA). Following three washes for 5–15 min each with 0.1% T-TBS (Tris buffered saline with Tween) buffer, the membranes were incubated with horseradish peroxidase-conjugated secondary anti-goat antibody (1:25000, Santa Cruz Biotechnology, TX, USA). The immunocomplexes were visualized using a ChemiDoc Touch Imaging System (Bio-Rad Laboratories). Densitometry analysis was performed using Image Lab software (Bio-Rad Laboratories).

2.6. RNA-seq analysis

For RNA-seq analysis of the SN, the PFF-injected and non-injected sides of the brain samples including the SN were analyzed. First, SAMR1 (N = 4) and SAMP8 (N = 4) mice were deeply anesthetized and perfused transcardially with PBS at 12 weeks post-injection. The brains were removed immediately and sectioned into five serial 1 mm-thick coronal block slices using a mouse brain matrix (RBM-2000C; ASI Instruments, MI, USA). Total RNA was isolated from frozen brain samples using a miRNeasy Mini Kit (QIAGEN, Hilden, Germany), according to the manufacturer’s instructions. The sample quality was estimated using a bioanalyzer 2100 (Agilent Technologies, CA, USA). RNA-seq libraries were generated using a TruSeq Stranded mRNA kit (Illumina, CA, USA). The pooled libraries were sequenced on an Illumina NovaSeq 6000 sequencer (101 base single-read mode, Illumina).

For gene expression analysis, the quality of the sequence reads was verified using FastQC version 0.11.8 (https://www.bioinformatics.babraham.ac.uk/projects/fastqc/). Adapter removal and quality trimming of sequence reads were performed using Trimmomatic version 0.36 (Bolger et al., 2014). The reads were aligned to the mouse reference genome (GRCm39) using STAR version 2.5.3a, and gene and isoform abundances were quantified using RSEM version 1.2.28 (Li and Dewey, 2011; Dobin et al., 2013). Differential expression analyses were conducted using Deseq2, version 1.34.0 (Love et al., 2014). Differentially expressed genes were defined using the Benjamin-Hochberg false discovery rate approach (adjusted P-value <0.05, absolute value of log2-fold change >2).

2.7. Statistical analysis

Histological quantification of p-α-syn positive areas, Iba1-positive and TH-positive cell counts, and western blotting were performed using GraphPad Prism version 9 (GraphPad Software, CA, USA). P values < 0.05 were considered statistically significant. The p-α-syn positive areas were analyzed using the nonparametric Mann-Whitney *U* test. Tukey’s multiple comparison tests were employed to analyze of the results of the TH- and Iba1-positive cells counts. Western blot was analyzed via Tukey’s multiple comparison test.

3. Results

3.1. SAMP8 mice injected with PFF exhibited significantly higher α-synucleinopathy than SAMR1 mice injected with PFF

We conducted immunohistochemical studies to evaluate the effects of senescence on Lewy pathology in the brains of PFF-injected mice. At 24 weeks after PFF injection into the SN, we detected p-α-syn positive Lewy pathology in the PFF-injected brains of both SAMR1 and SAMP8 mice. In contrast, no Lewy pathology was found in the saline-injected brains of SAMP8 or SAMR1 mice (Fig. 1, Supplementary Fig. 1A). Upon measuring the area of p-α-syn positive Lewy pathology in the SN, we observed that PFF-injected SAMP8 mice exhibited significantly stronger Lewy pathology than PFF-injected SAMR1 mice ($P = 0.0005$, 0.0214, respectively, Fig. 1A).

3.2. Exacerbated degeneration of nigrostriatal dopaminergic neurons in PFF-injected SAMP8 mice

To evaluate the effects of senescence on dopaminergic neurodegeneration, we stained and quantified the number of TH-positive dopaminergic neurons 24 weeks after PFF injection (Fig. 1B, Supplementary Fig. 1B). The saline-injected mice did not exhibit any signs of dopaminergic neurodegeneration. In contrast, SAMR1 and SAMP8 mice in which PFF was injected into the SN unilaterally exhibited significant dopaminergic neuronal cell loss compared with saline-injected mice ($P = 0.0003$ and $P < 0.0001$, respectively, Fig. 1B). PFF-injected SAMP8 mice exhibited significantly higher TH neuronal loss than PFF-injected SAMR1 mice in the injected side of the SN ($P = 0.0006$, Fig. 1B). We did not observe any significant differences in the number of TH positive cells in the non-injected side of the SN between groups (Fig. 1B).

Western blot analysis showed that TH protein levels in the SN were significantly lower in PFF-injected SAMP8 mice than in saline-injected

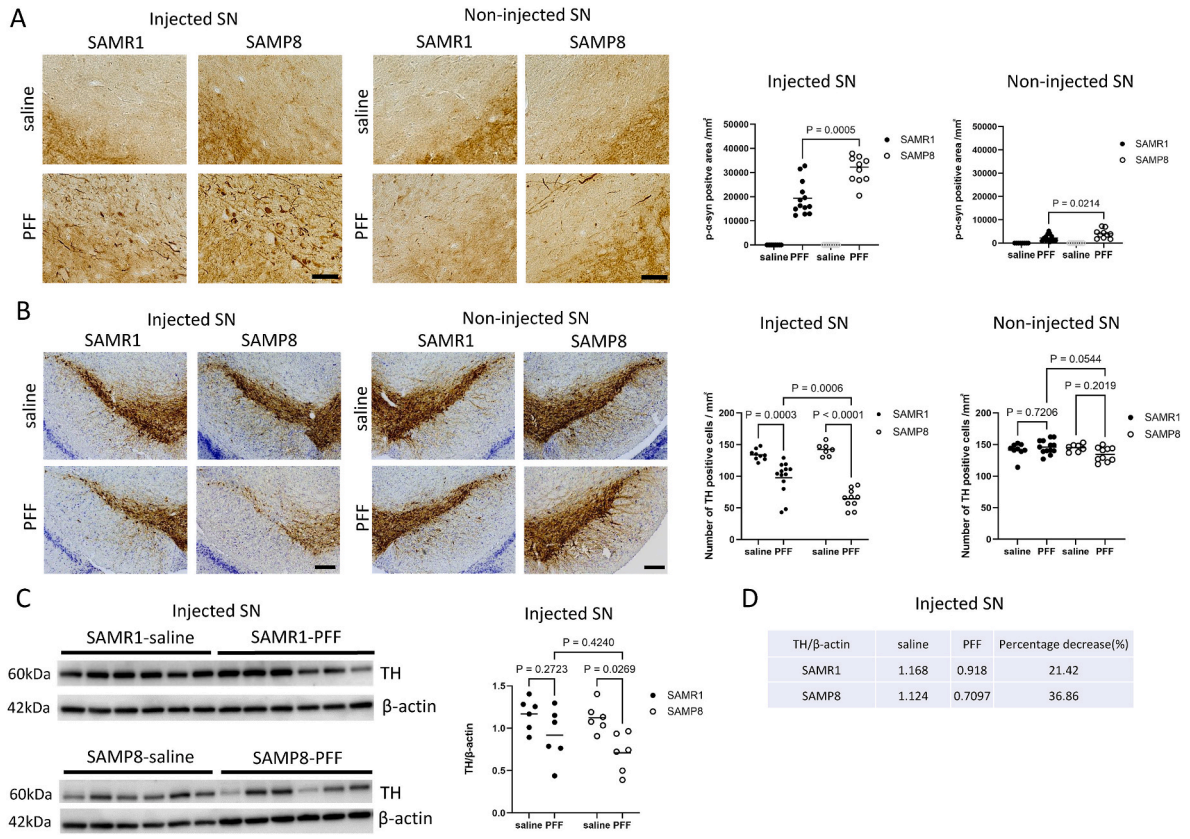

Fig. 1. 32-week-old SAMP8 mice exhibit severe p-α-syn pathology and dopaminergic neurons loss. (A) Representative images of p-α-syn pathology in the SN of SAMR1 and SAMP8 mice at 24 weeks after intranigral saline injection or PFF injection. Scale bar: 50 μm. Scatter plots presenting p-α-syn positive areas per mm^2 in the SN for each group; SAMR1-saline (N = 8), SAMR1-PFF (N = 13), SAMP8-saline (N = 7), SAMP8-PFF (N = 10). Horizontal bars in graphs represent the mean values. P value was obtained using the nonparametric Mann-Whitney *U* test. (B) Representative images of immunostaining for TH and counterstaining with Nissl in the SN of SAMR1 and SAMP8 mice 24 weeks after intranigral PFF or saline injection. Scale bar: 200 μm. Scatter plots indicating TH positive cell counts per mm^2 in the SN for each group; SAMR1-saline (N = 8), SAMR1-PFF (N = 13), SAMP8-saline (N = 7), SAMP8-PFF (N = 10). Horizontal bars in graphs represent the mean values. P values were obtained using Tukey's multiple comparison test. (C) Western blot analysis of TH obtained from the saline- or the PFF-injected side of SN in each group. β-actin is used as a loading control. Scatter plots of quantification of TH/β-actin in each group (N = 6). Horizontal bars in a graph represent mean values. (D) Table generated from the mean values of scatter plots in each group indicating the ratio of reduction of TH protein induced by PFF injection. P values were obtained using Tukey's multiple comparison test. α-syn, α-synuclein; p-α-syn, phosphorylated α-synuclein; SN, substantia nigra; PFF, α-synuclein preformed fibrils; SAMR1, senescence-accelerated resistant 1; SAMP8, senescence-accelerated prone 8.

SAMP8 mice (P = 0.0269, Fig. 1C). TH protein levels in the SN appeared to be lower in PFF-injected SAMR1 mice than in saline-injected SAMR1 mice, but the difference was not significant (P = 0.2723, Fig. 1C). TH protein levels in the SN appeared to be lower in PFF-injected SAMP8 mice than in PFF-injected SAMR1 mice, but the difference was not significant (P = 0.4240, Fig. 1C). SAMP8 mice showed a pronounced reduction in TH protein following PFF injection compared to SAMR1 mice (Fig. 1D).

3.3. *Persistent neuroinflammation in the substantia nigra of PFF-injected SAMP8 mice*

We evaluated neuroinflammation in each group by quantifying Iba1-positive cells using immunostaining. At 24 weeks after injection, Iba1-positive cells were significantly increased in the injected side of the SN in PFF-injected SAMP8 mice compared to that in saline-injected SAMP8 mice (P < 0.0001, Fig. 2A). Comparing the two PFF-injected groups, we detected a significant increase in Iba1-positive cells in SAMP8 mice compared to SAMR1 mice (P = 0.0066, Fig. 2A). No significant differences in the number of Iba1-positive cells were observed for the non-injected side of the SN among the four groups (Fig. 2A). Western blot analysis confirmed that the level of Iba1 was significantly higher in PFF-injected SAMP8 mice than in PFF-injected SAMR1 mice (P < 0.0001, Fig. 2B). SAMP8 mice exhibited a pronounced increase in Iba1 protein following PFF injection than SAMR1 mice (Fig. 2C).

3.4. *Altered immune activation in the transcriptome of PFF-injected SAMP8 mice compared to PFF-injected SAMR1 mice*

We performed RNA sequencing of the PFF-injected and non-injected side of the SN to analyze the patterns of differentially expressed genes (DEGs) underlying the pathogenesis of PFF injection. First, DEG analysis was performed on the SN samples injected with PFF collected from SAMP8 and SAMR1 mice. Comparative analysis revealed 178 DEGs (adjusted P value < 0.05, log2 fold change >2), of which 111 were upregulated and 67 were downregulated in the SAMP8 group (Supplementary Table 1, Fig. 3A). Second, DEG analysis was performed on the non-injected side of the SN. We identified 165 DEGs, of which 103 genes were upregulated and 62 were downregulated in the SAMP8 mice (Supplementary Table 2, Fig. 3B). Among the upregulated DEGs, 31 genes were exclusively identified in the former group but not in the latter (Supplementary Table 3, Fig. 3C and D). These 31 genes are thought to be affected by PFF injection and senescence via neuroinflammation. Notably, several of these genes, including CCL21 (Gm13304), IRF7, and HCAR2 are associated with neuroinflammation (Chen et al., 2002; Fu et al., 2015; Xu et al., 2021).

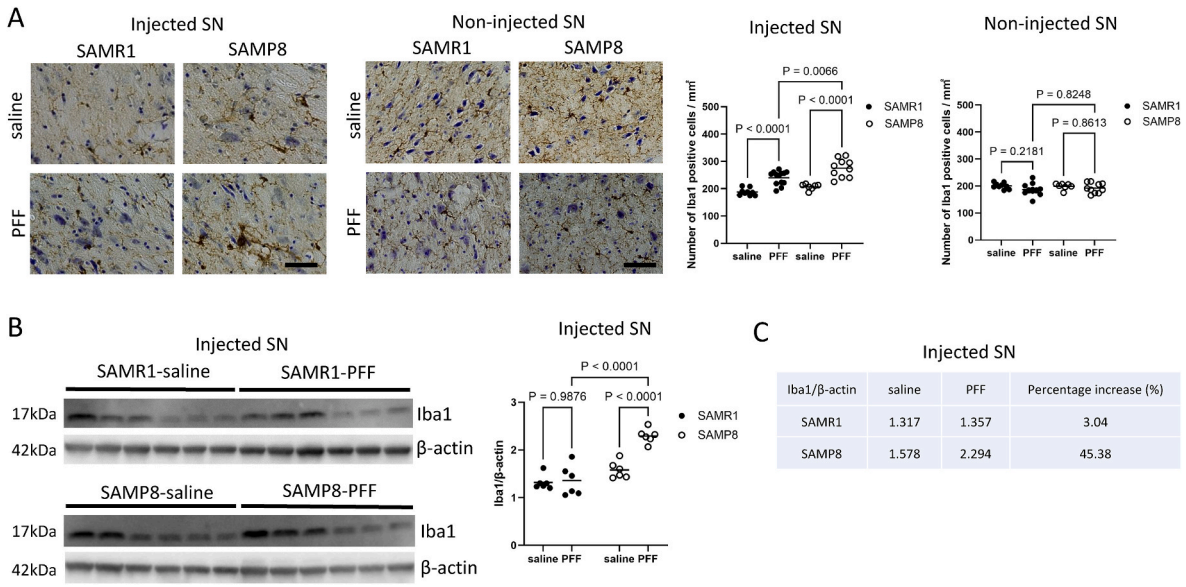

Iba1/β-actin	saline	PFF	Percentage increase (%)
SAMR1	1.317	1.357	3.04
SAMP8	1.578	2.294	45.38

Fig. 2. PFF injection induces a higher level of neuroinflammation in 32-week-old SAMP8 mice. (A) Representative images of Iba1 staining of the SN in each group. Scale bar: 50 μm. Scatter plots indicating Iba1 positive cell counts per mm^2 in the SN in each group; SAMR1-saline (N = 8), SAMR1-PFF (N = 13), SAMP8-saline (N = 7), SAMP8-PFF (N = 10). The horizontal bars in graphs represent the mean values. P values are obtained using Tukey's multiple comparison test. (B) Western blot analysis of Iba1 expression in the saline- or the PFF-injected side of the SN for each group (N = 6). β-actin was used as a loading control. Scatter plots depicting Iba1/β-actin quantification in each group. The horizontal bars represent the mean values. (C) Table generated from the mean values of scatter plots in each group indicating the ratio of increase of Iba1 protein induced by PFF injection in SAMR1 and SAMP8 mice. P values are obtained by Tukey's multiple comparison test. SN, substantia nigra; PFF, α-synuclein preformed fibrils; SAMR1, senescence-accelerated resistant 1; SAMP8, senescence-accelerated prone 8.

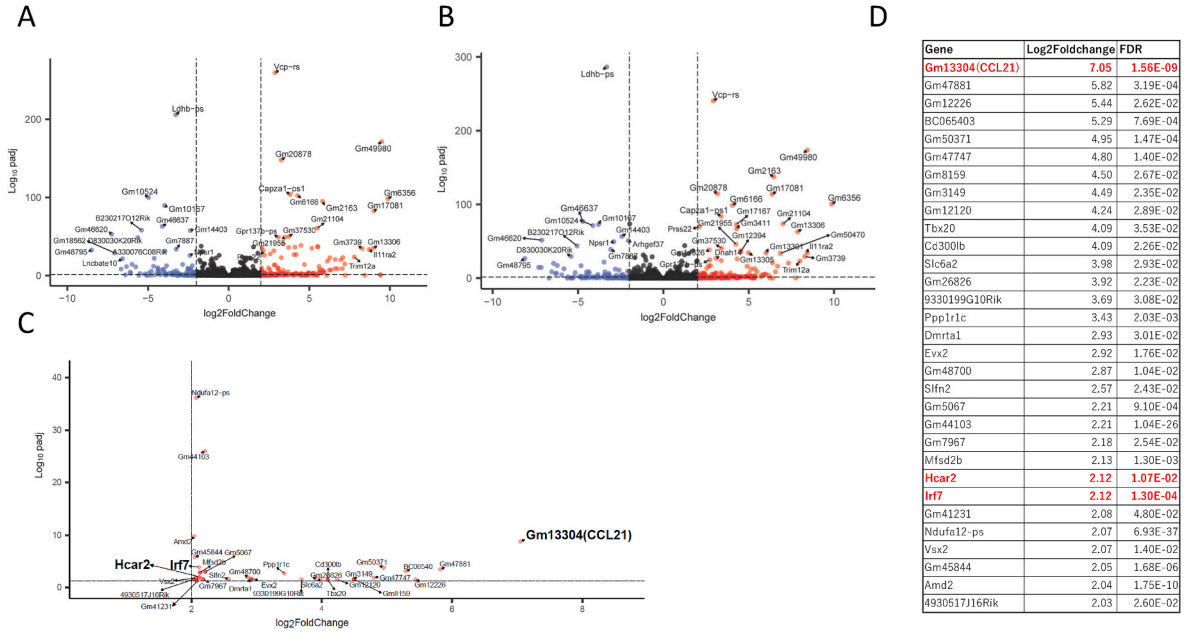

Gene	Log2Foldchange	FDR
Gm13304(CCL21)	7.05	1.56E-09
Gm47881	5.82	3.19E-04
Gm12226	5.44	2.62E-02
BC065403	5.29	7.69E-04
Gm50371	4.95	1.47E-04
Gm47747	4.80	1.40E-02
Gm8159	4.50	2.67E-02
Gm3149	4.49	2.35E-02
Gm12120	4.24	2.89E-02
Tbx20	4.09	3.53E-02
Cd300lb	4.09	2.26E-02
Slc6a2	3.98	2.93E-02
Gm26826	3.92	2.23E-02
9330199G10Rik	3.69	3.08E-02
Ppp1r1c	3.43	2.03E-03
Dmrta1	2.93	3.01E-02
Evx2	2.92	1.76E-02
Gm48700	2.87	1.04E-02
Slfn2	2.57	2.43E-02
Gm5067	2.21	9.10E-04
Gm44103	2.21	1.04E-26
Gm7967	2.18	2.54E-02
Mfsd2b	2.13	1.30E-03
Hcar2	2.12	1.07E-02
Irf7	2.12	1.30E-04
Gm41231	2.08	4.80E-02
Ndufa12-ps	2.07	6.93E-37
Vsx2	2.07	1.40E-02
Gm45844	2.05	1.68E-06
Amd2	2.04	1.75E-10
4930517J16Rik	2.03	2.60E-02

Fig. 3. RNA-seq analysis of the SN gene expression changes in 20-week-old SAMP8 (N = 4) and SAMR1 (N = 4) mice. (A) Volcano plot depicting differentially expressed genes (DEGs) between the SAMP8 and SAMR1 mice in the PFF-injected side. (B) Volcano plot showing DEGs between the SAMP8 and SAMR1 mice in the non-injected side. (C, D) Volcano plot and table showing significantly upregulated genes on the PFF-injected side excluding DEGs identified in the analysis of the non-injected side. SN, substantia nigra; PFF, α-synuclein preformed fibrils; SAMR1, senescence-accelerated resistant 1; SAMP8, senescence-accelerated prone 8.

3.5. CCL21-and Iba1-positive cells increased in PFF-injected SAMP8 mice

To validate our RNA sequencing result, we stained for CCL21 and analyzed the ratio of CCL21-positive Iba1-positive cells (microglia) and GFAP-positive cells (astrocyte) because CCL21 is an inflammatory cytokine present in glial cells and CCL21 showed the highest upregulation among altered genes (Fig. 3C). The ratio of CCL21-positive microglia did not increase in the SN of SAMR1 mice in response to PFF injection (Fig. 4A and C). On the other hand, the ratio of CCL21-positive microglia significantly increased in the SN of SAMP8 mice with PFF injection ($p < 0.0001$). Comparing PFF-injected SAMR1 and SAMP8 mice, CCL21-positive microglia were significantly increased in SAMP8 mice ($p < 0.0001$). The ratio of CCL21-positive astrocyte did not increase in the SN of SAMR1 and SAMP8 mice in response to PFF injection (Fig. 4B and D). However, when we compared PFF-injected SAMR1 and SAMP8 mice, we observed a significant increase in CCL21-positive

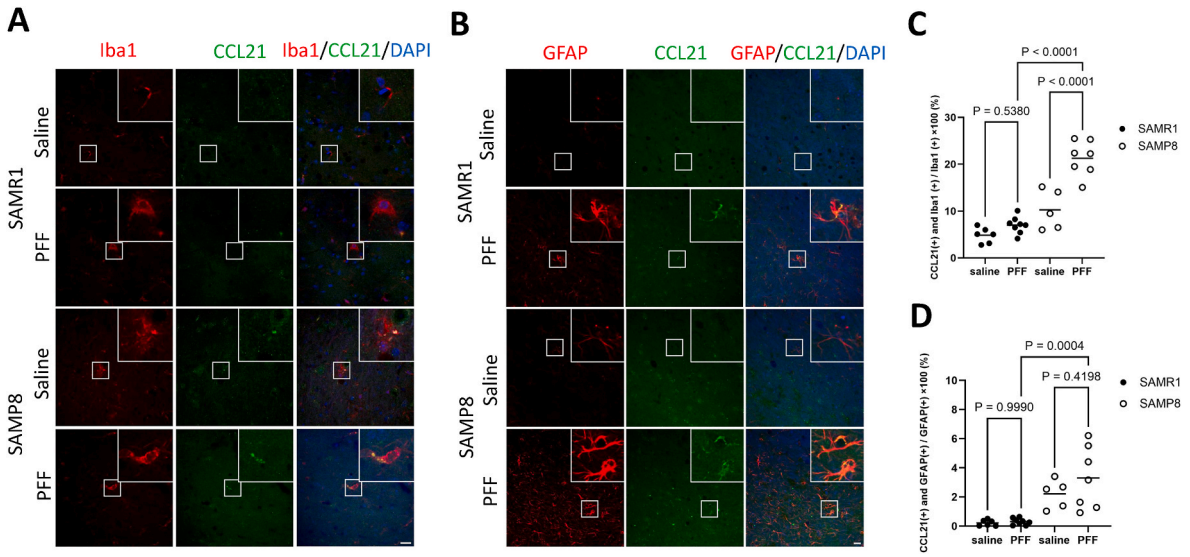

Fig. 4. Increased CCL21 signals in glial cells from 32-week-old SAMP8 mice injected with PFF. (A) Representative images of Iba1 and CCL21 double immunofluorescent staining in the injected side of the SN for each group. (red: Iba1, green: CCL21, blue: DAPI). (B) Representative images of GFAP and CCL21 double immunofluorescent staining in the injected side of the SN for each group. (red: GFAP, green: CCL21, blue: DAPI). (C) Scatter plots indicating the ratio of Iba1 positive area with CCL21 signal in Iba1 positive area in the SN in each group; SAMR1-saline (N = 6), SAMR1-PFF (N = 8), SAMP8-saline (N = 5), SAMP8-PFF (N = 7). The horizontal bars in graphs represent the mean values (SAMR1-saline, 4.85 %; SAMR1-PFF, 7.01 %; SAMP8-saline, 10.26 %; SAMP8-PFF, 21.27 %). P values are obtained using Tukey's multiple comparison test. (D) Scatter plots indicating the ration of GFAP positive- and CCL21-positive areas in GFAP positive areas in the SN in each group; SAMR1-saline (N = 6), SAMR1-PFF (N = 8), SAMP8-saline (N = 5), SAMP8-PFF (N = 7). The horizontal bars in graphs represent the mean values (SAMR1-saline, 0.22 %; SAMR1-PFF, 0.31 %; SAMP8-saline, 2.21 %; SAMP8-PFF, 3.31%). P values are obtained using Tukey's multiple comparison test. Scale bars: 20 μm. SN, substantia nigra; PFF, α-synuclein preformed fibrils; SAMR1, senescence-accelerated resistant 1; SAMP8, senescence-accelerated prone 8; DAPI, 4′,6-diamidino-2-phenylindole. (For interpretation of the references to colour in this figure legend, the reader is referred to the Web version of this article.)

astrocytes in SAMP8 mice ($p = 0.0004$).

We also evaluated IRF7 expression, as IRF7 is another inflammatory cytokine identified by RNA sequencing analysis (Fig. 3C). IRF7 signal was only slightly detected in Iba1-positive cells of SAMP8 mice. In contrast, we observed a substantial IRF7 signal in the GFAP-positive cells of the SAMP8 mice (Supplementary Fig. 2).

4. Discussion

In this study, we found that injecting PFF into the SN of SAMP8 mice results in robust p-α-syn pathology and more pronounced dopaminergic neurodegeneration than in SAMR1 mice. We further observed an increased number of Iba1-positive cells and levels of the inflammatory chemokine CCL21 in PFF-injected SAMP8 mice. These results suggest that accelerated senescence could exacerbate α-synuclein pathology, and one of the underlying mechanisms is accelerated senescence-mediated enhanced glial activation and cytokine-related pathways.

The present study demonstrated that PFF-induced p-α-syn positive Lewy pathology was more pronounced in SAMP8 mice, which are senescence-accelerated mice (Fig. 1A). Given that duplication of normal α-syn is known to cause PD, it is possible that changes in α-syn expression may have influenced the differential spread of the p-α-syn positive Lewy pathology shown in Fig. 1 (Chartier-Harlin M.C. et al., 2004). However, previous reports have indicated that α-syn expression was not significantly different between SAMP8 and SAMR1 mice at 2, 5, and 10 months of age, respectively (Kim H.S. et al., 2017). Therefore, it can be concluded that the present p-α-syn positive Lewy pathology results are not due to differences in α-syn expression. These results align with previous findings using a PFF-injected PD model in aged and young wild-type rats, demonstrating that aging promotes pathological p-α-syn propagation (Van den Berge et al., 2021). Regarding the PFF injection-induced dopaminergic neurodegeneration in the SN, SAMP8 mice exhibited a more advanced state than SAMR1 mice (Fig. 1B). Histological analysis showed a significant decrease in the number of TH-positive cells in PFF-injected SAMP8 mice; however, biochemical analysis did not show a significant reduction in TH protein levels (Fig. 1C and D). This discrepancy may be attributed to the differences in the analyzed samples: Western blot assay included not only the SN but also surrounding midbrain regions, which may result in decreased sensitivity to changes in TH protein levels. Nevertheless, our study revealed that accelerated senescence promotes pathological α-syn propagation and loss of dopaminergic neurons. Senescence causes biological events such as lysosomal dysfunction, increased oxidative stress, and chronic neuroinflammation, affecting protein folding (Saez-Atienzar and Masliah, 2020; Guerrero et al., 2021). As reported in previous studies, SAMP8 mice exhibit mitochondrial membrane rigidity, age-related autophagy-lysosomal alterations (García et al., 2011), and neuropathological changes, including amyloid-β deposition and elevated levels of hyperphosphorylated tau (Orejana et al., 2015; Li et al., 2023). Taken together, these senescence-related biological events in SAMP8 mice may contribute to the exacerbation of α-synucleinopathy and neurodegeneration.

Our study demonstrated a higher number of Iba1-positive cells in the PFF-injected SN in SAMP8 mice than in SAMR1 mice (Fig. 2A). Microglia are necessary for normal brain function; however, over-activated microglia cause severe neurotoxicity and neuroinflammation (Graeber and Streit, 2010). Neuroinflammation plays a significant role in senescence-associated central nervous system degeneration such as in PD (Hirsch and Hunot, 2009). Various studies using animal models of PD and postmortem examination of the brains of patients with PD have confirmed a significant association between microglial activation and dopaminergic neurodegeneration (Ouchi et al., 2005; Koprich et al., 2008). Furthermore, Gordon and colleagues reported that activation of the microglial inflammasome could drive α-syn propagation in PFF-injected mouse models (Gordon et al., 2018). Therefore, increased Iba1-positive microglia in PFF-injected SAMP8 mice may contribute to the exacerbated α-syn pathology and neuronal death observed in our study. SAMP8 mice are known to exhibit various aging-dependent neuroinflammation features, such as an increase in protein aggregates, the presence of Iba1-positive clusters, and an increase in the production

of pro-inflammatory cytokines such as IL-1β (Fernández et al., 2021). Observations from 3 to 9 months of age showed that plasma levels of TNFα and IL-6 were significantly elevated in SAMP8 mice compared to SAMR1 mice. Similarly, there was a significant increase in astrocytosis in the cerebral cortex and microgliosis in the brainstem of SAMP8 mice, whereas comparable changes were not observed in SAMR1 mice (Pačesová et al., 2022). In a previous study, aged SAMP8 mice treated with 1-methyl-4-phenyl-1,2,3,6-tetrahydropyridine (MPTP) exhibited more significant reductions in the number of dopaminergic neurons than young SAMP8 mice, as evidenced by an increase in microglial activation (Liu et al., 2010). The level of Iba1 protein that increases in response to PFF injections is significantly higher in SAMP8 mice than in SAMR1 mice (Fig. 2B and C). We consider these results to be consistent with previous findings suggesting that SAMP8 mice are more prone to neuroinflammation induced by PFF injections than SAMR1 mice. Taken together, the disruption of glial-mediated neuroinflammation with aging in SAMP8 mice, observed over 24 weeks after PFF injection, could result in exacerbated PD pathology.

To gain further insight into the molecular basis underlying exacerbated PD pathology in PFF-injected SAMP8 mice, we conducted a gene expression analysis. RNA sequencing revealed that various inflammation-related genes were upregulated in response to PFF injection in SAMP8 mice compared to those in SAMR1 mice (Fig. 3C and D). Among them was CCL21, a chemokine that plays an important role in brain damage by activating microglia. Previous studies have suggested that damaged neurons secrete CCL21 into the ischemic core after brain ischemia and injured spinal cord, leading to microglial activation through CXCR3 (Biber et al., 2001, 2007; De Jong et al., 2005; Zhao et al., 2007). In SAMP8 mice, the number of CCL21-positive microglia is increased by PFF injections. However, in SAMR1 mice, we could not observe any such changes regarding CCL21-positive microglia. (Fig. 4). Therefore, accelerated senescence can promote microglia activation via the CCL21-related pathway. We observed an increase in astrocytes considered to be reactive astrocytosis with PFF injection in both SAMP8 and SAMR1 mice, but the difference was not statistically significant. The injection of PFF did not raise the ratio of CCL21-positive astrocytes in both mice compared to each saline-injected group. The precise reason for this remains unclear, but it may be because the timing of the evaluation was delayed, occurring six months after the PFF injection. In a comparison of each PFF-injected groups, the ratio of increased CCL21-positive microglia and CCL21-positive astrocytes is higher in SAMP8 mice than in SAMR1 mice (Fig. 4C and D). This finding aligns with the RNA sequencing results (Fig. 3). Several studies have reported that CCL21 is expressed in microglia, while others have noted CCR7, the receptor for CCL21, expressed in astrocytes (Geraldo et al., 2023; Gomez-Nicola et al., 2010). Our results indicate CCL21 signaling overlaps with astrocytes, but further investigation is necessary to elucidate the details. Although it also remains unclear how CCL21 can enhance dopaminergic neurotoxicity in PFF-injected PD models, our result highlights the importance of CCL21 and related pathways in senescence and α-synucleinopathy. IRF7, the product of another gene upregulated by PFF in SAMP8 mice, is a transcription factor involved in immune responses and has been implicated in neuroinflammation. Through transcriptome sequencing, Li et al. demonstrated that IRF7 plays an important role in PD pathology and identified it as a key protein in protein-protein interactions in a rat model of PD (Li et al., 2019). Based on these previous reports, IRF7 activation could contribute to α-synucleinopathy by activating neurotoxic microglia. However, in this study, we could not confirm the IRF7 activation in microglia following PFF injection or accelerated senescence (Supplementary Fig. 2A). Tanaka et al. reported an increased expression of IRF7 during the M1-like microglial polarization switch, promoting neuroinflammation (Tanaka et al., 2015). IRF7 activation likely occurs at an early stage of neuroinflammation or shortly after PFF injection. Interestingly, we observed IRF7 activation in astrocytes in SAMP8 mice, with further enhancement by PFF injection (Supplementary Fig. 2B). The mechanism behind this activation remains unknown, but accelerated senescence may disrupt the IRF7 signal pathway, which may be more responsive to α-synucleinopathy, resulting in further exacerbation of neuroinflammation. HCAR2, also known as GPR109A, is a G-protein-coupled anti-inflammatory receptor. The anti-inflammatory effects of HCAR2 have been observed in a rat model of PD, and increased expression of HCAR2 has been found in the blood and the SN of patients with PD (Wakade et al., 2014; Fu et al., 2015), suggesting that SAMP8 miceinjected with PFF may exhibit the GPR109A overexpression. However, the GPR109A-mediated signaling pathway may be dysfunctional owing to impaired anti-inflammatory systems. In conclusion, the upregulation of these specific genes in PFF-injected SAMP8 mice may be linked to PD. Furthermore, given the association of these genes with inflammation-related processes, it can be inferred that accelerated senescence triggers neuroinflammation, thereby exacerbating the progression of PD through multiple pathways.

The present study has certain limitations regarding strains of mice used in experiments. Since the results of this study on dopaminergic neurodegeneration in SAMR1 mice were similar to our previous study on wild-type mice injected with PFF (Hayakawa et al., 2020), we hypothesize that the results in SAMP8 mice are due to accelerated senescence. Nevertheless, the absence of wild-type mice as a control group indicates that SAMR1 mice may have demonstrated a more pronounced protective effect against synucleinopathy than SAMP8 mice. Regarding RNA sequencing, it also remains possible that inflammation on the PFF-injected side may have spilled over to the contralateral side, or that ectopic transmission of PFF to the contralateral side via spinal fluid occurred, which may have affected the data for RNA sequencing. These points need to be further verified in the future.

5. Conclusion

This study demonstrated that PFF injection-induced PD pathology was more severe in SAMP8 mice than in SAMR1 mice. Accelerated senescence can promote α-synucleinopathy, progressive degeneration of dopaminergic neurons, and aberrant neuroinflammation. Furthermore, the PFF-injected SAMP8 mouse model was shown to be valuable to improve our understanding and control of the senescence process, potentially offering new pathways to control the progression of PD.

CRediT authorship contribution statement

Hiroshi Sakiyama: Writing – original draft, Validation, Investigation, Data curation. **Kousuke Baba:** Writing – review & editing, Writing – original draft, Validation, Supervision, Resources, Project administration, Methodology, Funding acquisition, Data curation, Conceptualization. **Yasuyoshi Kimura:** Writing – original draft, Validation, Supervision, Resources, Project administration, Methodology, Investigation, Formal analysis, Data curation. **Kotaro Ogawa:** Validation, Software, Resources, Methodology, Investigation, Formal analysis, Data curation. **Ujiakira Nishiike:** Resources, Methodology, Formal analysis, Data curation. **Hideki Hayakawa:** Resources, Methodology, Investigation, Formal analysis, Data curation. **Miki Yoshida:** Resources, Methodology, Investigation, Formal analysis, Data curation. **Cesar Aguirre:** Resources, Methodology. **Kensuke Ikenaka:** Validation, Supervision. **Seiichi Nagano:** Supervision, Funding acquisition. **Hideki Mochizuki:** Writing – original draft, Visualization, Funding acquisition, Conceptualization.

Data availability

The original contributions presented in this study are included in the article and supplementary material. Further inquiries can be directed to the corresponding author.

Funding

This work was supported by a JSPS KAKENHI Grant-in-Aid for Scientific Research (C) (20K07903 to HH and JP20K07865 to KB), Grant-in-Aid for Early-Career Scientists (JP20K16576 to HS), and Brain Mapping by Integrated Neurotechnologies for Disease Studies (Brain/MINDS) from the Japan Agency for Medical Research and Development (AMED JP19dm0207070 to HM).

Declaration of competing interest

The authors declare that they have no known competing financial interests or personal relationships that could have appeared to influence the work reported in this paper.

Acknowledgements

We would like to express our sincere appreciation to the Institute of Experimental Animal Sciences Faculty of Medicine staff for their cooperation in the breeding and management of the mice. We would like to thank Editage (www.editage.jp) for English language editing.

Appendix A. Supplementary data

Supplementary data to this article can be found online at https://doi.org/10.1016/j.neuint.2024.105906.

Data availability

Data will be made available on request.

References

Akiguchi, I., Pallàs, M., Budka, H., et al., 2017. SAMP8 mice as a neuropathological model of accelerated brain aging and dementia: toshio Takeda's legacy and future directions. Neuropathology 37, 293–305. https://doi.org/10.1111/neup.12373.

Baker, DJ, Petersen, RC., 2018. Cellular senescence in brain aging and neurodegenerative diseases: evidence and perspectives. J. Clin. Invest. 128, 1208–1216. https://doi.org/10.1172/JCI95145.

Barrientos, R.M., Kitt, M.M., Watkins, L.R., 2015. Neuroinflammation in the normal aging hippocampus. Neuroscience 309, 84–99. https://doi.org/10.1016/j.neuroscience.2015.03.007.

Biber, K., Neumann, H., Inoue, K., et al., 2007. Neuronal "On" and "Off" signals control microglia. Trends Neurosci. 30, 596–602. https://doi.org/10.1016/j.tins.2007.08.007.

Biber, K., Sauter, A., Brouwer, N., et al., 2001. Ischemia-induced neuronal expression of the microglia attracting chemokine secondary lymphoid-tissue chemokine (SLC). Glia 34, 121–133. https://doi.org/10.1002/glia.1047.

Bolger, A.M., Lohse, M., Usadel, B., 2014. Trimmomatic: a flexible trimmer for Illumina sequence data. Bioinformatics 30, 2114–2120. https://doi.org/10.1093/bioinformatics/btu170.

Bose, A., Beal, M.F., 2016. Mitochondrial dysfunction in Parkinson's disease. J. Neurochem. 139, 216–231. https://doi.org/10.1111/jnc.13731.

Chartier-Harlin, M.C., Kachergus, J., Roumier, C., et al., 2004. Alpha-synuclein locus duplication as a cause of familial Parkinson's disease. Lancet 364, 1167–1169. https://doi.org/10.1016/S0140-6736(04)17103-1.

Chen, S.-C., Leach, M.W., Chen, Y., et al., 2002. Central nervous system inflammation and neurological disease in transgenic mice expressing the CC chemokine CCL21 in oligodendrocytes. J. Immunol. 168, 1009–1017. https://doi.org/10.4049/jimmunol.168.3.1009.

Chinta, S.J., Woods, G., Demaria, et al., 2018. Cellular senescence is induced by the environmental neurotoxin paraquat and contributes to neuropathology linked to Parkinson's disease. Cell Rep. 22, 930–940. https://doi.org/10.1016/j.celrep.2017.12.092.

De Jong, E.K., Dijkstra, I.M., Hensens, M., 2005. Vesicle-mediated transport and release of CCL21 in endangered neurons: a possible explanation for microglia activation remote from a primary lesion. J. Neurosci. 25, 7548–7557. https://doi.org/10.1523/JNEUROSCI.1019-05.2005.

Dobin, A., Davis, C.A., Schlesinger, F., et al., 2013. STAR: ultrafast universal RNA-seq aligner. Bioinformatics 29, 15–21. https://doi.org/10.1093/bioinformatics/bts635.

Fernández, A., Quintana, E., Velasco, P., et al., 2021. Senescent accelerated prone 8 (SAMP8) mice as a model of age dependent neuroinflammation. J. Neuroinflammation 18, 1–20. https://doi.org/10.1186/s12974-021-02104-3.

Fu, S.P., Wang, J.F., Xue, W.J., et al., 2015. Anti-inflammatory effects of BHBA in both in vivo and in vitro Parkinson's disease models are mediated by GPR109A-dependent mechanisms. J. Neuroinflammation 12, 9. https://doi.org/10.1186/s12974-014-0230-3.

García, J.J., Piñol-Ripoll, G., Martínez-Ballarín, E., et al., 2011. Melatonin reduces membrane rigidity and oxidative damage in the brain of SAMP 8 mice. Neurobiol. Aging 32, 2045–2054. https://doi.org/10.1016/j.neurobiolaging.2009.12.013.

Geraldo, L.H., Garcia, C., Xu, Y., et al., 2023. CCL21-CCR7 signaling promotes microglia/macrophage recruitment and chemotherapy resistance in glioblastoma. Cell. Mol. Life Sci. 280, 179. https://doi.org/10.1007/s00018-023-04788-7.

Gomez-Nicola, D., Pallas-Bazarra, N., Valle-Argos, B., et al., 2010. CCR7 is expressed in astrocytes and upregulated after an inflammatory injury. J. Neuroimmunol. 227, 87–92. https://doi.org/10.1016/j.jneuroim.2010.06.018.

Gordon, R., Albornoz, E.A., Christie, D.C., et al., 2018. Inflammasome inhibition prevents -synuclein pathology and dopaminergic neurodegeneration in mice. Sci. Transl. Med. 10, eaah4066. https://doi.org/10.1126/scitranslmed.aah4066.

Graeber, M.B., Streit, W.J., 2010. Microglia: biology and pathology. Acta Neuropathol. 119, 89–105. https://doi.org/10.1007/s00401-009-0622-0.

Guerrero, A., De Strooper, B., Arancibia-Cárcamo, I.L., 2021. Cellular senescence at the crossroads of inflammation and Alzheimer's disease. Trends. Neurosci 44, 714–727. https://doi.org/10.1016/j.tins.2021.06.007.

Hayakawa, H., Nakatani, R., Ikenaka, K., et al., 2020. Structurally distinct α-synuclein fibrils induce robust parkinsonian pathology. Mov. Disord. 35, 256–267. https://doi.org/10.1002/mds.27887.

Hirsch, E.C., Hunot, S., 2009. Neuroinflammation in Parkinson's disease: a target for neuroprotection? Lancet Neurol. 8, 382–397. https://doi.org/10.1016/S1474-4422(09)70062-6.

Kaushik, S., Cuervo, A.M., 2015. Proteostasis and aging. Nat. Med. 21, 1406–1415. https://doi.org/10.1038/nm.4001.

Kempster, P.A., O'Sullivan, S.S., Holton, J.L., et al., 2010. Relationships between age and late progression of Parkinson's disease: a clinico-pathological study. Brain 133, 1755–1762. https://doi.org/10.1093/brain/awq059.

Kim, H.S., Moon, S., Kim, S., et al., 2017. Chronological changes in the expression of phosphorylated tau and 5-AMP-activated protein kinase in the brain of senescence-accelerated P8 mice. Mol. Med. Rep. 15, 3301–3309. https://doi.org/10.3892/mmr.2017.6361.

Koprich, J.B., Reske-Nielsen, C., Mithal, P., et al., 2008. Neuroinflammation mediated by IL-1β increases susceptibility of dopamine neurons to degeneration in an animal model of Parkinson's disease. J. Neuroinflammation 5, 1–12. https://doi.org/10.1186/1742-2094-5-8.

Li, B., Dewey, C.N., 2011. RSEM: accurate transcript quantification from RNA-Seq data with or without a reference genome. BMC Bioinf. 12, 323. https://doi.org/10.1186/1471-2105-12-323.

Li, B., Li, J., Hao, Y., et al., 2023. Yuanzhi Powder inhibits tau pathology in SAMP8 mice: mechanism research of a traditional Chinese formula against Alzheimer's disease. J. Ethnopharmacol. 311, 116393. https://doi.org/10.1016/j.jep.2023.116393.

Li, J., Sun, Y., Chen, J., 2019. Transcriptome sequencing in a 6-hydroxydopamine rat model of Parkinson's disease. Genes Genet. Syst. 94, 61–69. https://doi.org/10.1266/ggs.18-00036.

Liu, B., Liu, J., Shi, J.-S., 2020. SAMP8 mice as a model of age-related cognition decline with underlying mechanisms in Alzheimer's disease. J. Alzheim. Dis. 75, 385–395. https://doi.org/10.3233/jad-200063.

Liu, J., Wang, M.W., Gu, P., et al., 2010. Microglial activation and age-related dopaminergic neurodegeneration in MPTP-treated SAMP8 mice. Brain Res. 1345, 213–220. https://doi.org/10.1016/j.brainres.2010.05.043.

Love, M.I., Huber, W., Anders, S., 2014. Moderated estimation of fold change and dispersion for RNA-seq data with DESeq2. Genome Biol. 15, 550. https://doi.org/10.1186/s13059-014-0550-8.

Martínez-Cué, C., Rueda, N., 2020. Cellular senescence in neurodegenerative diseases. Front. Cell. Neurosci. 14, 16. https://doi.org/10.3389/fncel.2020.00016.

Mogi, M., Harada, M., Kondo, T., et al., 1994. Interleukin-lfl, interleukin-6, epidermal growth factor and transforming growth factor-are elevated in the brain from parkinsonian patients. Neurosci. Lett. 180, 147–150. https://doi.org/10.1016/0304-3940(94)90508-8.

Orejana, L., Barros-Miñones, L., Jordan, J., et al., 2015. Sildenafil decreases BACE1 and cathepsin B levels and reduces APP amyloidogenic processing in the SAMP8 mouse. Gerontol. A Biol. Sci. Med. Sci. 70, 675–685. https://doi.org/10.1093/gerona/glu106.

Ouchi, Y., Yoshikawa, E., Sekine, Y., et al., 2005. Microglial activation and dopamine terminal loss in early Parkinson's disease. Ann. Neurol. 57, 168–175. https://doi.org/10.1002/ana.20338.

Pačesová, A., Holubová, M., Hrubá, L., et al., 2022. Age-related metabolic and neurodegenerative changes in SAMP8 mice. Aging 14, 7300–7327. https://doi.org/10.18632/aging.204284.

Pringsheim, T., Jette, N., Frolkis, A., et al., 2014. The prevalence of Parkinson's disease: a systematic review and meta-analysis. Mov. Disord. 29, 1583–1590. https://doi.org/10.1002/mds.25945.

Ray Dorsey, E., Elbaz, A., Nichols, E., et al., 2018. Global, regional, and national burden of Parkinson's disease, 1990–2016: a systematic analysis for the Global Burden of Disease Study 2016. Lancet Neurol. 17, 939–953. https://doi.org/10.1016/S1474-4422(18)30295-3.

Reale, M., Costantini, E., Aielli, L., et al., 2022. Proteomic signature and mRNA expression in hippocampus of SAMP8 and SAMR1 mice during aging. Int. J. Mol. Sci. 23, 15097. https://doi.org/10.3390/ijms232315097.

Rodriguez, M., Rodriguez-Sabate, C., Morales, I., et al., 2015. Parkinson's disease as a result of aging. Aging Cell 14, 293–308. https://doi.org/10.1111/acel.12312.

Saez-Atienzar, S., Masliah, E., 2020. Cellular senescence and Alzheimer disease: the egg and the chicken scenario. Nat. Rev. Neurosci. 21, 433–444. https://doi.org/10.1038/s41583-020-0325-z.

Spillantini, M.G., Schmidt, M.L., Lee, V.M., et al., 1997. Alpha-synuclein in Lewy bodies. Nature 388, 839–840. https://doi.org/10.1038/42166.

Tanaka, T., Murakami, K., Bando, Y., et al., 2015. Interferon regulatory factor 7 participates in the M1-like microglial polarization switch. Glia 63, 595–610. https://doi.org/10.1002/glia.22770.

Tofaris, G.K., Goedert, M., Spillantini, M.G., 2017. The transcellular propagation and intracellular trafficking of α-synuclein. Cold Spring Harb Perspect Med. 7. https://doi.org/10.1101/cshperspect.a024380.

Van den Berge, N., Ferreira, N., Mikkelsen, T.W., et al., 2021. Ageing promotes pathological alpha-synuclein propagation and autonomic dysfunction in wild-type rats. Brain 144, 1853–1868. https://doi.org/10.1093/brain/awab061.

Wakade, C., Chong, R., Bradley, E., et al., 2014. Upregulation of GPR109A in Parkinson's disease. PLoS One 9, e109818. https://doi.org/10.1371/journal.pone.0109818.

Wirdefeldt, K., Adami, H.O., Cole, P., et al., 2011. Epidemiology and etiology of Parkinson's disease: a review of the evidence. Eur. J. Epidemiol. 26, S1–S58. https://doi.org/10.1007/s10654-011-9581-6.

Wood, S.J., Wypych, J., Steavenson, S., et al., 1999. alpha-synuclein fibrillogenesis is nucleation-dependent. Implications for the pathogenesis of Parkinson's disease. J. Biol. Chem. 274, 19509–19512. https://doi.org/10.1074/jbc.274.28.19509.

Xu, S., Mei, S., Lu, J., et al., 2021. Transcriptome analysis of microglia reveals that the TLR2/IRF7 signaling axis mediates neuroinflammation after subarachnoid hemorrhage. Front. Aging Neurosci. 13, 645649. https://doi.org/10.3389/fnagi.2021.645649.

Yagi, H., Kusaka, E., Hongo, K., et al., 2005. Amyloid fibril formation of α-synuclein is accelerated by preformed amyloid seeds of other proteins: implications for the mechanism of transmissible conformational diseases. J. Biol. Chem. 280, 38609–38616. https://doi.org/10.1074/jbc.M508623200.

Zhao, P., Waxman, S.G., Hains, B.C., 2007. Modulation of thalamic nociceptive processing after spinal cord injury through remote activation of thalamic microglia by cysteine-cysteine chemokine ligand 21. J. Neurosci. 27, 8893–8902. https://doi.org/10.1523/JNEUROSCI.2209-07.2007.